An Optimal Dispatching Algorithm of Microgrid Based on Improved Particle Filter

Yi Wang, Ying Cai, Zhen Chang, Yanling Shang, Fangzheng Gao, and Quan Sun

***Abstract*—To enhance the operational economy and energy utilization efficiency of the microgrid, this paper takes the minimization of the comprehensive cost of microgrid operation and environmental protection as the objective function and constructs the microgrid power dispatching model including wind and solar, gas, diesel power generation and energy storage units. By using an improved Sparrow Search Algorithm (ISSA) to optimize the particle filter algorithm, an improved particle filter (IPF) algorithm is developed for microgrid optimization scheduling strategies. Simulation examples demonstrate that, compared to traditional SSA and ISSA algorithms, the proposed algorithm has the advantages of shorter computation time and higher solution accuracy, which also proves its strong practicability in the microgrid optimal dispatching.**

***Index Terms*—microgrid; optimal dispatch; multi-objective optimization; improved particle filter**

I. Introduction

Under the dual impetus of the "dual carbon" goals and the principles of energy conservation and emission reduction, green and sustainable development has become the key direction of the accelerated transformation of power grids. However, the operation of power grids inevitably leads to energy waste and reduced economic efficiency, making the optimization of the energy structure in power grids a matter of paramount importance [1,2]. Microgrids, as an essential means of promoting the utilization of renewable energy, can save energy and improve efficiency through well-designed systems paired with optimized algorithms. Currently, experts in this field have conducted extensive discussions and research on how to optimize microgrid performance from multiple perspectives [3-5].

The following is a summary of a series of studies conducted by experts in the field regarding microgrid modeling. Ref. [6] focuses on the simplified modeling of microgrids, reducing them to systems composed of multiple micro-source inverters, ensuring the stability of the AC bus voltage and frequency. This model serves as a foundation for designing control strategies for microgrids and is of great significance in voltage and frequency regulation during transitions between grid-connected and islanded modes. Ref. [7] introduces distributed generation units, such as photovoltaic energy, energy storage systems, and small hydropower, into the microgrid model, combining both linear and nonlinear control strategies. This significantly improves the system's ability to regulate and respond under complex operating conditions. In Ref. [8], an equivalent structural model of the microgrid is established, and a novel phase-locked loop (PLL) structure is designed to enhance phase-locking accuracy under grid voltage distortion. This modeling approach effectively reduces voltage transients during grid connection and improves system stability.

Focusing on the current development of multi-objective optimization in microgrids, Ref. [9] combines the particle swarm optimization (PSO) algorithm with the artificial hummingbird algorithm (AHA), forming the PSO-AHA algorithm to solve microgrid problems. The research findings indicate that the PSO-AHA-tuned STATCOM effectively improves the voltage recovery capability of the microgrid, enhancing the system's robustness and stability. Ref. [10] emphasizes the application of the sparrow search algorithm (SSA) in microgrids. By simulating the foraging behavior of sparrows, SSA optimally reallocates single-phase loads based on objective functions of voltage and current imbalance. Compared with traditional methods, SSA reduces the number of load switches while maintaining load balancing effectiveness. Ref. [11] proposes a microgrid optimization scheduling strategy based on an improved sparrow search algorithm (ISSA). By incorporating Logistic-Circle chaotic mapping, the sea squirt optimization algorithm, dynamic inertia weight, water wave dynamic factors, and Cauchy-Gauss mutation strategies, the global and local search capabilities of the sparrow search algorithm are enhanced. Ref. [12] introduces an enhanced sparrow search algorithm (ESSA) that optimizes the economic dispatch of isolated microgrids by integrating elite opposition-based learning, elite guidance, and adaptive t-disruption mechanisms. However, the ESSA algorithm has some disadvantages. In

Manuscript received April 28, 2024; revised August 7, 2024. This work was partially supported by the National Natural Science Foundation of China under grant 61873120, the National Natural Science Foundation of Jiangsu Province under grants BK20201469 and BE2021016-5, the Postgraduate Research & Practice In-novation Program of Jiangsu Province under Grant SJCX 23_1181 and the Qing Lan project of Jiangsu Province.

Yi Wang is a postgraduate student in the School of Automation, Nanjing Institute of Technology, Nanjing 211167, China (email: y00450220120@njit.edu.cn).

Ying Cai is a postgraduate student in the School of Automation, Nanjing Institute of Technology, Nanjing 211167, China (email: y00450220407@njit.edu.cn).

Zhen Chang is a postgraduate student in the School of Automation, Nanjing Institute of Technology, Nanjing 211167, China (email: y00450220449@njit.edu.cn).

Yanling Shang is an associate professor in the School of Automation, Nanjing Institute of Technology, Nanjing 211167, China (e-mail: hnnhsyl@126.com).

Fangzheng Gao is a professor in the School of Automation, Nanjing Institute of Technology, Nanjing 211167, China (corresponding author, e-mail: gaofz@126.com).

Quan Sun is an associate professor in the School of Automation, Nanjing Institute of Technology, Nanjing 211167, China (e-mail: sunquan@126.com).

complex scenarios, it may converge prematurely or become trapped in local optima during later iterations. Additionally, the improvement mechanisms increase computational complexity, leading to higher demands on computational resources when handling large-scale problems.

Based on the aforementioned research, this paper constructs a microgrid power dispatch model that includes wind energy, solar energy, gas, diesel generation, and energy storage units. By using an improved sparrow search algorithm (ISSA) to optimize the particle filtering algorithm, an improved particle filtering (IPF) algorithm is proposed for the optimal scheduling of microgrids. This algorithm features shorter computation times and higher solution accuracy.

II. Microgrid System Economic Dispatch Model

In this chapter, we introduce the mathematical description of multi-objective optimal scheduling model of microgrid.

A. Microgrid System Model

Wind power model

The output power of a wind turbine is significantly influenced by wind speed. Specifically, a wind turbine generates electricity only when the wind speed falls within a certain range. The power output model is as follows:

$$P_{\mathrm{WI}}=\begin{cases}0 & v\le v_{ci},v\ge v_{\mathrm{co}}\\ \dfrac{v^3-v_{ci}^3}{v_{\mathrm{r}}^3-v_{ci}^3}P_{\mathrm{r}} & v_{ci}\le v\le v_{\mathrm{r}}\\ P_{\mathrm{r}} & v_{\mathrm{r}}\le v\le v_{\mathrm{co}}\end{cases} \tag{1}$$

here, v_{ci} is the cut-in wind speed, which is the minimum wind speed at which the wind turbine starts generating electricity; v_{co} is the cut-out wind speed, which is the wind speed above which the wind turbine stops generating electricity to protect itself; v_{r} is the rated wind speed, at which the wind turbine can achieve its maximum power output; P_{WI} is the actual power of the wind turbine; and P_r is the rated power of the wind turbine.

Photovoltaic (*PV*) power generation mathematical model

Photovoltaic (*PV*) cells convert light energy directly into electrical energy. Their output power is greatly influenced by environmental conditions and exhibits significant nonlinear characteristics. The power output model for photovoltaic generation is as follows:

$$P_{PV}=q\cdot P_{rated}\cdot\left(\frac{G}{G_{stc}}\right)\cdot(1+\alpha_{PV}(T-T_{stc})) \tag{2}$$

where q is the derating factor of the photovoltaic cell, typically taken as 0.8; P_{rated} is the rated output power of the photovoltaic cell; G is the actual solar irradiance; G_{stc} is the solar irradiance under standard test conditions; α_{PV} is the temperature coefficient of the photovoltaic cell; T is the current cell temperature; and T_{stc} is the cell temperature under standard test conditions. This model reflects the characteristics of photovoltaic cell output power as it varies with changes in irradiance and temperature.

Micro gas turbine model

Microturbines, as a type of distributed power source, have fuel cost and efficiency as their primary performance indicators. The model for a microturbine is as follows:

$$F_{MT}=C\cdot\frac{1}{\mathrm{LHV}}\frac{P_{MT}}{\eta_{MT}} \tag{3}$$

$$\eta_{MT}=a+b\cdot P_{MT}+c\cdot P_{MT}^2+d\cdot P_{MT}^3 \tag{4}$$

in these formulas, F_{MT} is the fuel cost of the microturbine, C is the natural gas price, P_{MT} is the output power of the microturbine, and η_{MT} is the efficiency of the microturbine, which is a cubic function of the output power P_{MT}. To accurately describe the efficiency curve of the microturbine, the parameters a, b, c and d are assigned the following values: a=30, b=2, c=1.7, and d=0.0301. These parameters are obtained by fitting the actual performance data of the microturbine and can accurately reflect the efficiency variation of the microturbine at different output power levels. In this paper, C is set to 2 yuan/m^3, and the Lower Heating Value (*LHV*) is set to 9.7 kWh/m^3.

Diesel generator model

Diesel engines are commonly used in fuel generators, and their operation involves various costs, including fuel expenses, maintenance costs, and pollutant treatment fees[13]. These costs are significant and cannot be ignored in the operation of diesel generators. The specific model for diesel engine power generation is as follows:

$$\begin{cases}C_{\mathrm{DE.OM}}(t)=K_{\mathrm{DE.OM}}P_{\mathrm{DE}}(t)\\ C_{\mathrm{DE.F}}(t)=\alpha P_{\mathrm{DE}}^2(t)+\beta P_{\mathrm{DE}}(t)+\gamma\\ C_{\mathrm{DE.EN}}(t)=\sum_{k=1}^{n}(C_k\gamma_{\mathrm{de},k})P_{\mathrm{DE}}(t)\end{cases} \tag{5}$$

where $C_{\mathrm{DE.OM}}(t)$, $C_{\mathrm{DE.F}}(t)$, and $C_{\mathrm{DE.EN}}(t)$ represent the operation and maintenance cost, fuel cost, and pollutant treatment cost of the diesel engine at time t, respectively; $P_{\mathrm{DE}}(t)$ is the power generation of the diesel engine at time t; $K_{\mathrm{DE.OM}}$ is the operation and maintenance cost coefficient of the diesel engine; $\gamma_{\mathrm{de},k}$ is the emission amount of pollutant k produced by the operation of the diesel engine; and C_k is the cost coefficient for pollutant treatment. The parameters are set as follows: α =0.00011, β =0.1801, and γ =6.

Battery model

Batteries play a crucial role in microgrid systems by regulating the balance between power supply and demand through the charging and discharging process, thereby mitigating the uncertainty of wind and solar energy outputs. Specifically, the charging and discharging state of the battery can be described by the following formulas:

$$E_{SB}(t)=E_{SB}(t-1)+\left(\frac{P_{total}(t)-P_{load}(t)}{\eta_{inv}\cdot\eta_{sb}}\right) \tag{6}$$

where $E_{SB}(t)$ represents the capacity of the battery at time *t*. $E_{SB}(t-1)$ represents the capacity of the battery at time *t-1*. $P_{total}(t)$ is the total output of the microgrid at time *t*. $P_{load}(t)$ is the total load of the system at time *t*. η_{inv} is the efficiency of the inverter. η_{sb} is the efficiency of the battery's charge and discharge, and the definitions of above symbols can be found in [6-12].

B. Microgrid Costs and Objective Function

To ensure the economic efficiency, reliability, and environmental sustainability of microgrid operation, this paper establishes a multi-objective optimization scheduling model that comprehensively considers various costs within the microgrid system. The model includes the operational costs and environmental protection costs of the microgrid[14]. The operational costs cover the total costs of interactions between the microgrid and the main grid, maintenance costs of energy storage, total operational costs of microturbines, and total operational costs of diesel generators. The environmental protection costs mainly consider the pollutant treatment costs of the main grid and the pollutant emission treatment cost coefficients during operation. This paper comprehensively considers the microgrid system and solves the model under four scenarios: minimum environmental protection cost, minimum system operational cost, minimum total cost, and a compromise solution, to achieve dual optimization of economic and environmental performance of the system[15].

Microgrid operating costs

Let $C_g(t)$, $C_{bs}(t)$, $C_{MT}(t)$, and $C_{DE}(t)$ represent the total interaction cost, storage maintenance cost, microturbine total cost, and diesel generator operating cost at time t, respectively. Let $P_{bs}(t)$, $P_{sl}(t)$, $P_b(t)$, $C_b(t)$, and $C_{sl}(t)$ represent the storage power, power sold by the microgrid to the main grid, power purchased from the main grid, and the buying and selling prices of electricity between the microgrid and the main grid at time t.

The modeling of microgrid operating costs is as follows:

$$f_1 = \sum_{t=1}^{T} C_g(t) + C_{MT}(t) + C_{DE}(t) \tag{7}$$

$$\begin{cases} C_g(t) = C_b(t) + C_{sl}(t) \\ C_b(t) = c_b(t) P_b(t) \\ C_{sl}(t) = c_{sl}(t) P_{sl}(t) \\ C_{DE}(t) = C_{DE.OM}(t) + C_{DE.F}(t) \\ C_{MT}(t) = C_{MT.OM}(t) + C_{MT.F}(t) \end{cases} \tag{8}$$

Microgrid environmental costs

Environmental costs mainly consider the treatment costs for the emissions of CO_2, SO_2, and NO_x from the units. Clean energy sources such as PV and WT do not need to account for environmental costs as they do not produce pollutant gases during operation. Let $C_{G.EN}(t)$ be the pollutant treatment cost of the main grid at time t; $\gamma_{g,k}$ be the emission amount of pollutant k produced by the main grid; and C_k be the cost coefficient for treating pollutant k.

The environmental protection cost of the microgrid is as follows:

$$\begin{cases} f_2 = \sum_{t=1}^{T} C_{G.EN}(t) + C_{MT.EN}(t) + C_{DE.EN}(t) \\ C_{G.EN}(t) = \sum_{k=1}^{n} (C_k \gamma_{g,k}) P_b(t) \end{cases} \tag{9}$$

Objective function of microgrid dispatch model

The purpose of the microgrid scheduling model is to minimize the total cost, which includes both the microgrid operating costs and the environmental protection costs. Therefore, the objective function is defined as follows:

$$Z = f_1 + f_2 \tag{10}$$

where Z represents the total cost of the microgrid.

C. Microgrid Constraints

System power balance constraint

$$P_{load}(t) = P_{WT}(t) + P_{PV}(t) + P_{MT}(t) + P_{bs}(t) + P_{DE}(t) + P_g(t) \tag{11}$$

Where $P_{WT}(t)$ is the output power of the wind turbine, $P_{PV}(t)$ is the output power of the photovoltaic cells, $P_{MT}(t)$ is the active output power of the microturbine, $P_{bs}(t)$ is the charging and discharging power of the battery, $P_{DE}(t)$ is the diesel generator power, and $P_g(t)$ is the total interaction cost between the microgrid and the main grid.

Microturbine output constraints

$$\begin{cases} P_{MT,\min}(t) \le P_{MT}(t) \le P_{MT,\max}(t) \\ \left| P_{MT}(t) - P_{MT}(t-1) \right| \le r_{MT} \\ Q_{MT,\min}(t) \le Q_{MT}(t) \le Q_{MT,\max}(t) \\ Q^{co}_{MT,\min}(t) \le Q^{co}_{MT}(t) \le Q^{co}_{MT,\max}(t) \\ Q^{he}_{MT,\min}(t) \le Q^{he}_{MT}(t) \le Q^{he}_{MT,\max}(t) \end{cases} \tag{12}$$

where $P_{MT,min}(t)$ and $P_{MT,max}(t)$ represent the minimum and maximum power of the microturbine, $P_{MT}(t-1)$ represents the active output power of the microturbine at time $t-1$, r_{MT} represents the ramp rate constraint of the microturbine, $Q_{MT}(t)$ represents the thermal output of the microturbine at time t, $Q_{MT,min}(t)$ and $Q_{MT,max}(t)$ represent the lower and upper limits of the thermal output of the microturbine, respectively; $Q^{co}_{MT}(t)$ represents the cooling output of the microturbine at time t, $Q^{co}_{MT,\min}(t)$ and $Q^{co}_{MT,\max}(t)$ represent the lower and upper limits of the cooling output of the microturbine; $Q^{he}_{MT}(t)$ represents the heating output of the microturbine at time t; $Q^{he}_{MT,\min}(t)$ and $Q^{he}_{MT,\max}(t)$ represent the lower and upper limits of the heating output of the microturbine at time t.

Diesel generator output constraints

$$\begin{cases} P^{\min}_{DE}(t) \le P_{DE}(t) \le P^{\max}_{DE}(t) \\ \left| P_{DE}(t) - P_{DE}(t-1) \right| \le r_{DE} \end{cases} \tag{13}$$

where $P^{\min}_{DE}(t)$ and $P^{\max}_{DE}(t)$ represent the minimum and maximum power of the diesel generator, $P_{DE}(t-1)$ represents the power of the diesel generator at time $t-1$, and r_{DE} represents the ramp rate constraint of the diesel generator.

Microgrid line transmission power constraints

$$P^{\min}_g(t) \le P_g(t) \le P^{\max}_g(t) \tag{14}$$

where $P^{\min}_g(t)$ and $P^{\max}_g(t)$ represent the lower and upper limits of the transmission power of the microgrid line, respectively.

Battery operation constraints

$$\begin{cases} p^{\min}_{bs}(t) \le p_{bs}(t) \le p^{\max}_{bs}(t) \\ E^{\min}_{bs}(t) \le E_{bs}(t) \le E^{\max}_{bs}(t) \end{cases} \tag{15}$$

where $p^{\min}_{bs}(t)$ and $p^{\max}_{bs}(t)$ represent the lower and upper limits of the charging and discharging power of the battery, $E_{bs}(t)$ represents the energy storage capacity of the battery, and $E^{\min}_{bs}(t)$ and $E^{\max}_{bs}(t)$ represent the lower and upper limits of the battery's energy storage capacity.

III. Improved Particle Filter Algorithm

A. Sparrow Search Algorithm

To improve the particle filter algorithm's performance, this paper introduces a bio-inspired optimization technique to enhance the sampling process.

The Sparrow Search Algorithm, inspired by sparrow foraging and anti-predation behaviors, operates based on the following fitness value matrix:

$$F_x = [f(x_1), f(x_2), \cdots, f(x_N)]^T \tag{16}$$

$$f(x_i) = [f(x_{i,1}), f(x_{i,2}), \cdots f(x_{i,d})] \tag{17}$$

where N is the size of the sparrow population, and d is the dimension.

The sparrow population is divided into three roles: discoverers, followers, and vigilantes. Discoverers are individuals with high fitness values and have a larger search range compared to other individuals. Their position update method is shown in the following formula:

$$X_{i,j}^{t+1} = \begin{cases} X_{i,j}^{t} \cdot \exp(-\dfrac{i}{\alpha \cdot iter}), R_2 < ST \\ X_{i,j}^{k} + Q \cdot L, \qquad R_2 \geq ST \end{cases} \tag{18}$$

where i represents the *i-th* sparrow in the population $i = 1, 2, \cdots, n$; j represents the *j-th* dimension of the optimization problem $j = 1, 2, \cdots, d$; t represents the *t-th* iteration of the optimization algorithm; *iter* indicates the maximum number of iterations of the algorithm; α is a random value in the interval $(0,1]$; R_2 represents the early warning value in the process of foraging; *ST* represents the safety value in the process of foraging; Q is a random value following a normal distribution; L represents a matrix of $1 \times D$. When $R_2 < ST$, the sparrow population is in a safe environment, and the discoverers should continue to expand their search range. Otherwise, it indicates the presence of predators in the surrounding environment, and the population should move to a safe area for foraging.

When the sparrow population is foraging, followers in the population will follow the discoverers, and their position is updated as follows:

$$X_{i,j}^{t+1} = \begin{cases} Q \cdot \exp(\dfrac{X_{worst} - X_{i,j}^{t}}{i^2}), & i > \dfrac{n}{2} \\ X_p^{t+1} + \left| X_{i,j}^{t} - X_p^{t+1} \right| \cdot A^{+} \cdot L, & i \leq \dfrac{n}{2} \end{cases} \tag{19}$$

where X_{worst} represents the worst position of the sparrow in the population; X_p represents the optimal position reached by the discoverer in the population; A represents a matrix of $1 \times D$, where the elements are randomly 1 or -1, $A^{+} = A^{T}(AA^{T})^{-1}$; When $i > n/2$, it means that the follower did not capture the food that the discoverer was seeking and needs to move to other areas to continue foraging.

During the foraging process, some sparrows are selected as vigilantes to handle reconnaissance and provide early warning about the surrounding environment. When predators appear, vigilantes abandon their current food and move toward other sparrows to avoid danger. Vigilantes usually make up 10%-20% of the entire population, and their positions are updated as follows:

$$X_{i,j}^{t+1} = \begin{cases} X_{best}^{t} + \beta \cdot \left| X_{i,j}^{t} - X_{best}^{t} \right|, f_i > f_g \\ X_{i,j}^{t} + k \dfrac{\left| X_{i,j}^{t} - X_{worst}^{t} \right|}{f_i - f_w + \varepsilon}, \quad f_i = f_g \end{cases} \tag{20}$$

where X_{best} represents the best position of the current sparrow population; β is a random value that follows a normal distribution and is used to control the movement step of the sparrow individual; k is a random number used to control the moving direction and distance of individual sparrows, ranging from $[-1,1]$; i represents the *i-th* fitness value of the sparrow in the population; f_g and f_w represent the fitness values of the global optimal and worst positions, respectively. The constant ε is included to avoid division by 0. When $f_i > f_g$, it indicates the approach of natural enemies in the surrounding environment; when $f_i = f_g$, sparrows move closer to other individuals to avoid danger.

B. Improved Sparrow Search Algorithm

Aiming at the defects of the sparrow search algorithm, such as poor population diversity and a tendency to fall into local optima, this paper proposes a multi-strategy improved sparrow search algorithm.

(1) Optimize population diversity by chaotic mapping

Studies have shown that the initial population distribution in bionic optimization algorithms significantly impacts their optimization performance. A more uniform initial distribution leads to better search speed and optimization results. Using chaotic maps to optimize the initial population positions can enhance diversity without altering the population's randomness. Research indicates that, among commonly used chaotic models, the Sin chaotic model offers superior chaotic characteristics compared to the Logistic chaotic model due to its infinite number of mapping folds. Therefore, this paper employs the Sin chaotic model to optimize the population diversity in the sparrow search algorithm. The expression is shown in formula (21):

$$\begin{cases} x_{n+1} = \sin \dfrac{2}{x_n}, n = 0, 1, \cdots, N \\ -1 \leq x_n \leq 1, \quad x_n \neq 0 \end{cases} \tag{21}$$

(2) Improve SSA search strategy

The original SSA search strategy can be divided into two situations: approaching the origin and jumping to the position of the optimal solution. These two strategies cause the SSA to easily fall into local optima and weaken its global search ability. To address these deficiencies, this paper improves the original SSA search strategy. First, the approach-to-origin strategy is removed. The position update method for the finder is then modified, as shown in formula (22):

$$x_{i,j}^{t+1} = \begin{cases} x_{i,j}^{t} \cdot (1 + \delta), R_2 < ST \\ x_{i,j}^{t} + \delta, \qquad R_2 \geq ST \end{cases} \tag{22}$$

where δ is a random value that follows a normal distribution.

Additionally, the position update method for vigilantes is modified. When a sparrow approaches other individuals to avoid danger, if it is in the optimal position of the current population, it will randomly move between the optimal and worst positions of the population. If the sparrow is not in the optimal position, it will move randomly between its current position and the population's optimal position. The improved position update method for vigilantes is shown as:

$$X_{i,j}^{t+1} = \begin{cases} X_{i,j}^{t} + \beta \cdot \left| X_{i,j}^{t} - X_{best}^{t} \right|, & f_i > f_g \\ X_{i,j}^{t} + \beta \cdot \left| X_{worst}^{t} - X_{best}^{t} \right|, & f_i = f_g \end{cases} \tag{23}$$

(3) Introduce the Cauchy-Gaussian mutation strategy

In the later stages of the original SSA iteration, it often falls into local optima. To mitigate this, the Cauchy-Gaussian

mutation strategy is employed to mutate the individual with the best fitness value in the current population. The values before and after the mutation are compared, and the better position is selected for the next iteration. The specific formula is as follows:

$$L_{best}^{t} = X_{best}^{t}\left[1+\eta_1 cauchy\left(0,\sigma^2\right)+\eta_2 gauss\left(0,\sigma^2\right)\right] \quad (24)$$

$$\sigma = \begin{cases} 1, & f(X_{best}) < f(X_i) \\ \exp\left(\dfrac{f(X_{best})-f(X_i)}{\left|f(X_{best})\right|}\right), & f(X_{best}) > f(X_i) \end{cases} \quad (25)$$

where L_{best}^{t} is the position of the optimal individual in the population after mutation; σ^2 is the standard deviation of the Cauchy-Gaussian mutation strategy; $cauchy(0,\sigma^2)$ and $gauss(0,\sigma^2)$ are random variables satisfying Cauchy and Gaussian distribution; η_1 and η_2 are random numbers that obey the normal distribution.

The global search advantage of the Cauchy mutation strategy and the local search advantage of the Gaussian mutation is utilized to help the algorithm escape local optima while maintaining its global search capability.

C. Particle Filter Algorithm Based on ISSA Optimization

Traditional particle filters typically increase the number of particles to enhance sample diversity and delay particle degradation. However, an excessive number of particles can reduce the algorithm's efficiency, which is not suitable for applications like indoor positioning that require high real-time performance.

An effective proposed distribution can accurately represent the real distribution, ensuring sample rationality and diversity with fewer particles. This approach avoids particle degradation and divergence of filtering results, maintaining the effectiveness of the filtering algorithm.

This paper optimizes the particle filter sampling process using the Improved Sparrow Search Algorithm (ISSA). The specific process is as follows:

Step 1: Initialize relevant parameters, including the number of particles, population size, dimension, ratio of discoverers and vigilantes, and the maximum number of iterations.

Step 2: Using the fitness function $f(x_i)$, calculate the fitness value of each particle in the population. Sort the particles in ascending order based on their fitness values, and identify the particle with the best current fitness value.

Step 3: Select a certain proportion of particles as discoverers and update their positions according to formula (22). Then, select another proportion of particles as joiners and update their positions according to formula (23). Finally, randomly select a proportion of particles as vigilantes and update their positions according to formula (24).

Step 4: Obtain the new positions of all particles. Apply the Cauchy-Gaussian mutation strategy to mutate the individual with the best fitness value. Compare the positions before and after the mutation: if the new position is better, retain it; otherwise, keep the old position. Store the position with the best fitness value as X_{best}^{t} and record the corresponding fitness value.

Step 5: Check if the termination condition is met or if the maximum number of iterations is reached. If the condition is satisfied, output the optimal solution. If not, return to Step 2.

This optimization process concentrates the particles in high-likelihood areas, thereby reducing particle degradation and divergence in the filter.

D. Testing Functions

To validate the feasibility and superiority of the IPF algorithm proposed in this paper, four classic benchmark functions (denoted as $F_1 - F_4$) are selected to test SSA, ISSA, and the IPF. The formulas for the test functions are as follows:

$$F_1(x) = \sum_{i=1}^{D-1}[100(x_{i+1}-x_i^2)^2+(x_i-1)^2] \quad (26)$$

$$F_2(x) = \pi\{10\sin(\pi y_1)+\sum_{i=1}^{D-1}(y_i-1)^2[1+10\sin^2(\pi y_{i+1})]/D + (y_D-1)^2\}+\sum_{i=1}^{D}u(x_i,10,100,4) \quad (27)$$

$$F_3(x) = \sum_{i=1}^{11}\left[a_i - x_1(b_i^2+b_i x_2)/(b_i^2+b_i x_3+x_4)\right]^2 \quad (28)$$

$$F_4(x) = [1+(x_1+x_2+1)^2(19-14x_1+3x_1^2 -14x_2+6x_1x_2+3x_2^2)]\times[30+(2x_1-3x_2)^2 \times(18-32x_2+12x_1^2+48x_2-36x_1x_2+27x_2^2)] \quad (29)$$

The dimensions (D), variable ranges, and theoretical minimum values of the testing functions are presented in Table 1. The 3D views of the testing functions are illustrated in Figs. 1-4.

TABLE I
TESTING FUNCTIONS AND PARAMETERS

Function	D	Range	F_{min}
F_1	30	[-30,30]	0
F_2	30	[-50,50]	0
F_3	4	[-5,5]	0.00030
F_4	2	[-2,2]	3

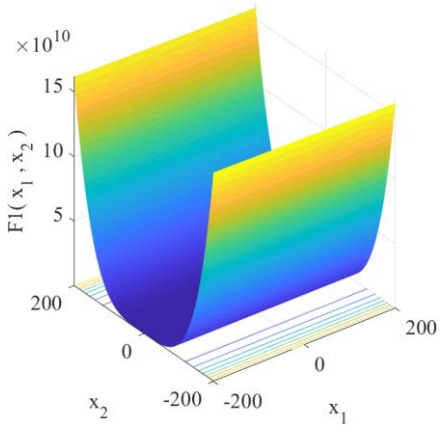

Fig. 1. 3D view of F_1

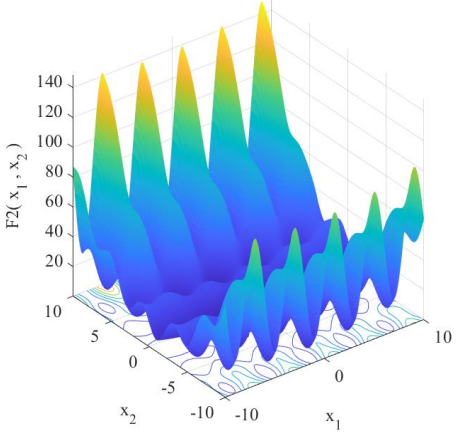

Fig. 2. 3D view of F_2

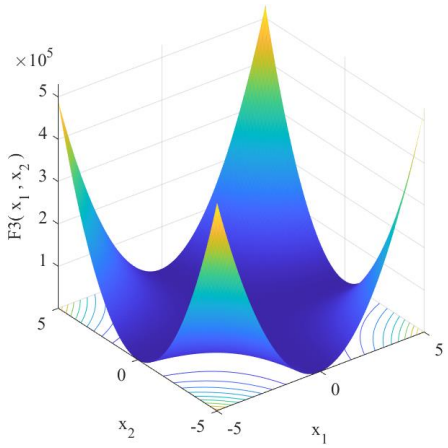

Fig. 3. 3D view of F3

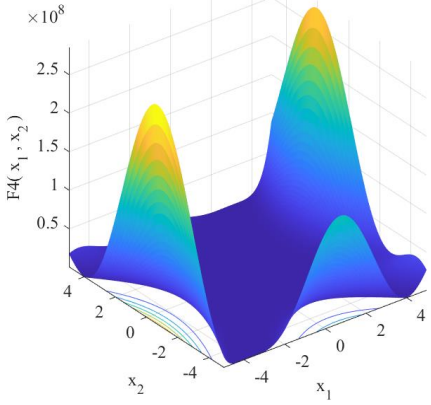

Fig. 4. 3D view of F4

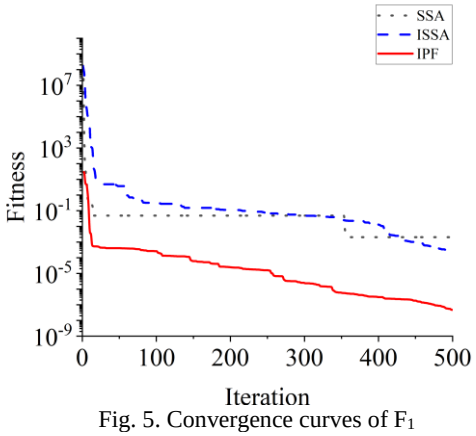

Fig. 5. Convergence curves of F1

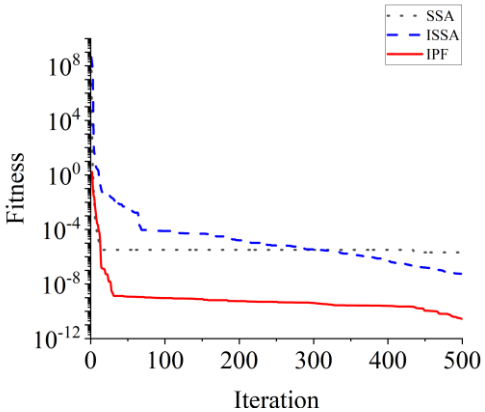

Fig. 6. Convergence curves of F2

To comprehensively evaluate the development and exploration capabilities of the IPF algorithm, Table 2 lists the average fitness and standard deviation results of SSA, ISSA, and IPF under benchmark functions. Figs. 5-8 compare the convergence curves of the three algorithms.

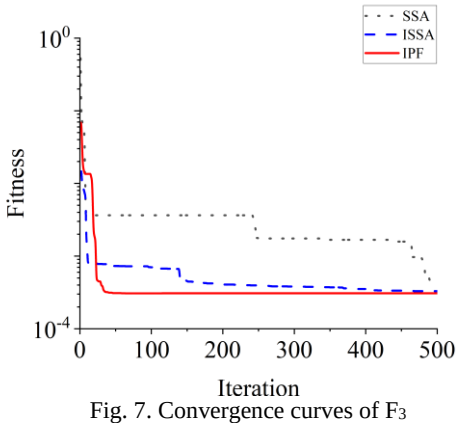

Fig. 7. Convergence curves of F3

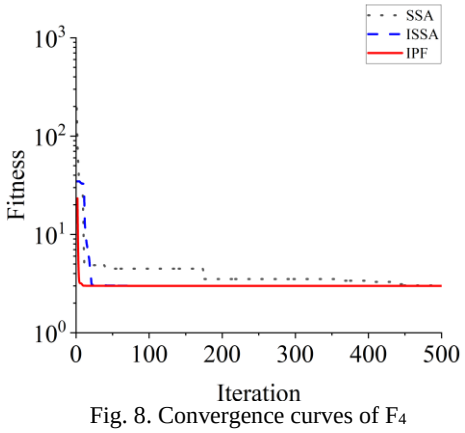

Fig. 8. Convergence curves of F4

TABLE 2
COMPARISON RESULTS

Function	Criteria	SSA	ISSA	Improved ISSA
F1	Avg	5.15E-03	4.77E-05	4.32E-05
	Std	1.51E-02	5.15E-06	9.12E-07
F2	Avg	4.15E-06	3.71E-08	5.25E-09
	Std	3.18E-06	1.88E-08	2.75E-09
F3	Avg	4.66E-04	4.18E-04	3.21E-04
	Std	1.19E-04	1.79E-04	6.21E-05
F4	Avg	3.04E+00	3.00E+00	3.00E+00
	Std	2.99E-02	5.57E-06	2.79E-08

From Table 2, it can be seen that the IPF outperforms both ISSA and SSA algorithms across the four test problems. For the unimodal function F_1, the IPF effectively searches for the global optimum, significantly enhancing the solution accuracy. In the case of the multimodal function F_2, the IPF demonstrates better average fitness and standard deviation compared to the SSA and the ISSA algorithms. Furthermore, in the tests of the fixed-dimensional multimodal functions F_3 and F_4, the IPF exhibits exceptional robustness. This is due to the IPF's use of chaotic mapping to optimize population diversity, the enhancement of search strategies, and the introduction of the Cauchy-Gaussian mutation strategy, which significantly boosts its global search capability and solution accuracy. The convergence curves in Figs. 5-8 visually illustrate the superiority of the IPF algorithm in problem-solving.

IV. CASE ANALYSIS

Consider that the microgrid includes multiple distributed energy sources such as photovoltaic (PV), wind turbines (WT), micro gas turbines (MT), and diesel engines (DE). The related parameters of this microgrid are listed in Tables 3-6.

TABLE 3
UNIT PARAMETERS

Equipment	Power Range (Kw)	Maximum Ramp-Up Power (Kw/min)	Unit Price for O&M(yuan/Kwh)
WT	[0,90]	0	0
PV	[0,60]	0	0
MT	[2,30]	1.7	0.0301
DE	[6,36]	1.6	0.139
Grid	[-30,30]	0	0

TABLE 4
POLLUTANT EMISSION COEFFICIENTS AND COSTS

Name	Cost (yuan/kg)	Pollutant Emission Coefficient (g/Kwh)				
		WT	PV	MT	DE	Grid
SO2	5	0	0	0.003	0.299	2
NOX	7	0	0	1.3	12	1.8
CO2	0.021	0	0	700	650	900

TABLE 5
BATTERY PARAMETERS

Equipment	Parameter	Value
Battery	Maxi Capacity(kWh)	150
	Mini Capacity(kWh)	5
	Maxi Input Power(kW)	30
	Max Output Power(kWh)	30
	Initial Capacity(kW)	20
	Charge and Discharge Rate	0.9

TABLE 6
TIME-OF-USE ELECTRICITY PRICES

Type	Time		Price
Sell	Peak	10:00~14:00 18:00~22:00	1.35
	Mid-Peak	07:00~09:00 15:00~17:00	0.82
	Off-Peak	00:00~06:00 23:00~24:00	0.38
Purchase	All-Day	00:00~24:00	0.36

To analyze the scenarios with the lowest operating costs, lowest environmental protection costs, and lowest total costs, this paper also addresses the power distribution under a compromise solution. The process of selecting the compromise solution includes the following steps:

(1) Normalization of Objective Functions. Normalize the operating costs and environmental protection costs of the non-dominated solutions to facilitate comparison. The normalization formula is as follows:

$$f_i' = \frac{f_i}{\max(f_i)}, \quad i = 1,2 \tag{30}$$

(2) Weighted Sum Method. Perform a weighted sum of the objective functions. Choose the solution with the smallest weighted sum as the compromise solution. The formula is as follows:

$$\text{object}(i) = f_1'(i) + f_2'(i) \tag{31}$$

(3) Selecting the Optimal Solution. Choose the solution with the smallest comprehensive objective value as the compromise solution.

By following these steps, an effective balance between multiple objective functions can be achieved, which leads to the identification of a compromise solution to optimize the scheduling of the microgrid.

TABLE 7
ALGORITHM COMPARATIVE ANALYSIS

	SSA	ISSA	IPF
Number of iterations	100	100	100
Iteration time(s)	349	333	298
Optimal value(yuan)	1556.3	1495.5	1409.8
Average(yuan)	1605.5	1544.7	1477.6

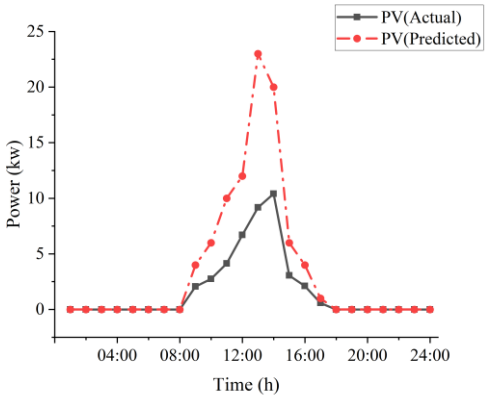

Fig. 9. Predicted and actual photovoltaic power

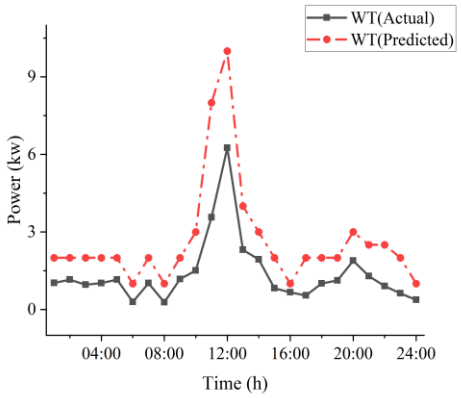

Fig. 10. Predicted and actual wind power

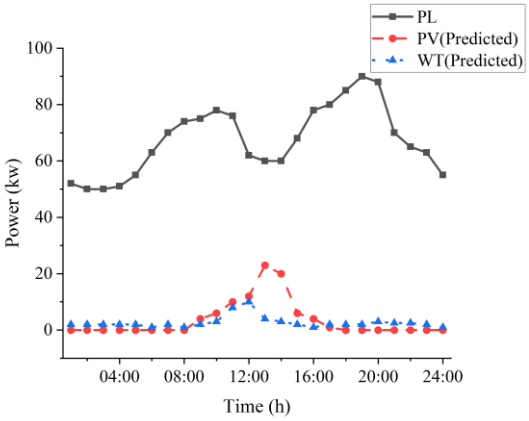

Fig. 11. Predicted photovoltaic, wind power, and total load

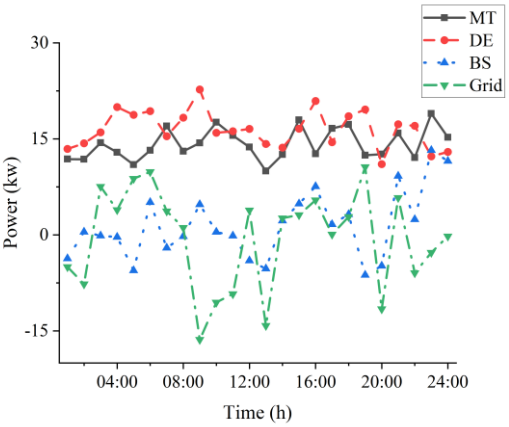

Fig. 12. Compromise solution

By setting the number of iterations to 100, the average iteration time, optimal value, and mean value of 10 experimental results were recorded. From Table 7, it can be

seen that the iteration time of the IPF algorithm is 14.6% and 10.5% faster than that of the SSA and ISSA algorithms, respectively. The optimal and average microgrid cost values obtained by the IPF are significantly better than those computed by the SSA and ISSA. In terms of optimal value, the IPF is 9.4% and 5.7% lower than the SSA and ISSA, respectively; in terms of average value, the IPF is 8.0% and 4.3% lower than the SSA and ISSA, respectively. Therefore, it can be concluded that compared to SSA and ISSA, the IPF algorithm achieves higher solution accuracy and faster speed for the microgrid problem discussed in this paper.

Fig.9 illustrates the actual and predicted photovoltaic power. Fig.10 depicts the actual and predicted wind power. Fig. 11 shows the predicted photovoltaic power, predicted wind power, and microgrid load power.

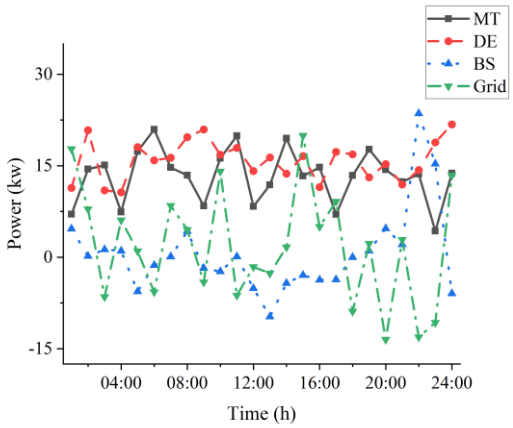

Fig. 13. Minimum total cost solution

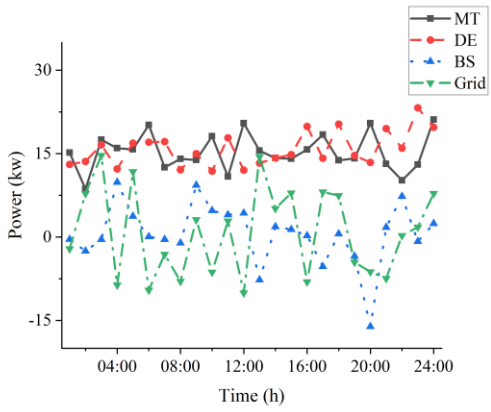

Fig. 14. Minimum operating cost solution

The optimization scheduling model proposed in this paper aims to minimize microgrid costs. The total microgrid cost includes operating costs and environmental costs, with a weighted sum of these two forming the compromise scenario. To evaluate the impact of the objective functions on the scheduling results, this paper discusses the scheduling results when different objective functions are used. Fig 12 shows the power distribution in the compromise scenario, Fig 13 depicts the power distribution when the total cost is minimized, Fig 14 illustrates the power distribution when the operating cost is minimized, and Fig 15 displays the power distribution when the environmental cost is minimized.

A simple energy analysis reveals that the battery storage (BS) acts as an auxiliary regulator, with its charging and discharging strategy adjusted according to changes in electricity prices. The battery charges when prices are low and discharges when prices are high, thereby reducing the economic and environmental costs of the microgrid. Since photovoltaic and wind power generation cannot fully meet the load demand, the microgrid must purchase electricity from the main grid and rely on distributed energy sources to meet the load demand.

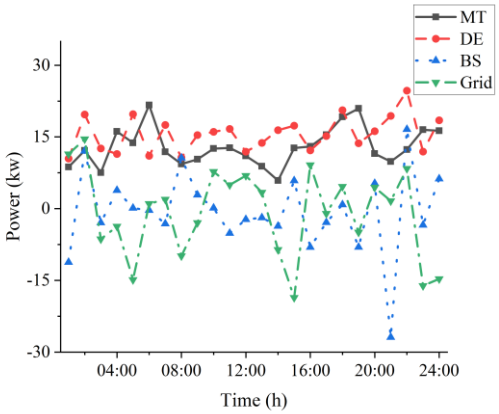

Fig. 15. Minimum environmental protection cost solution

V. Conclusions

This paper has taken the minimization of the comprehensive cost of microgrid operation and environmental protection as the objective function and constructs the microgrid power dispatching model including wind and solar, gas, diesel power generation and energy storage units. And an improved particle filter algorithm for microgrid optimal dispatching strategy has been obtained. Simulation examples show that the iteration time of the proposed IPF algorithm is 14.6% faster than that of the SSA and 10.5% faster than that of the ISSA. In terms of optimal value, the IPF algorithm is 9.4% lower than the SSA and 5.7% lower than the ISSA. And in terms of average value, the IPF algorithm is 8.0% lower than the SSA and 4.3% lower than the ISSA. These data fully demonstrate the superiority and efficiency of the IPF algorithm in microgrid optimization scheduling.

References

[1] S. Zhao, J. Wang, H. Wang, and A. He, "Control strategies of microgrid at micro-source level and system level," *Engineering Letters*, vol. 28, no.1, pp.155-167, 2020.

[2] J. Velez-Ramirez, and E Giraldo, "Hierarchical linear-nonlinear DC microgrid control,"*IAENG International Journal of Computer Science*, vol. 48, no.3, pp.456-462, 2021.

[3] X. Du, S. Zhao, J. Wang, A. He, "Design of double decoupled phase-locked loop of microgrid and smooth switching control strategy for on-grid and off-grid connection," *IAENG International Journal of Computer Science*, vol. 48, no.2, pp.392-405, 2021.

[4] X. Zhang, X. Zhu, D. Wu, Z. Xiao, Z. Tao, and H. Zhao, "Nonlinear features of bark wavelet sub-band filtering for pathological voice recognition," *Engineering Letters*, vol. 29, no.1, pp.49-60, 2021.

[5] Y. Zhang, L. Li, and W. Hu, "An integrated energy demand response model considering source-load synergy and stepped carbon trading mechanism," *Engineering Letters*, vol. 32, no. 3, pp.614-624, 2024.

[6] X. Zhao, Z. Zhang, Y. Xie, and M. Jin, "Economic-environmental dispatch of microgrid based on improved quantum particle swarm optimization," *Energy*, vol. 195, pp.117014, 2020.

[7] Q. Ahmed, K. Aziah, and G. Kim, "Optimal economic dispatch to minimize load shed-ding and operation cost for networked microgrids," *Arabian Journal for Science and Engineering*, vol. 48, no. 11, pp. 15419-15434, 2023.

[8] S. Said, A. Ali, and B. Hartmann, "Tie-line power flow control method for grid connected microgrids with SMES based on optimization and

fuzzy logic," *Journal of Modern Power Systems and Clean Energy*, vol. 8, no. 5, pp. 941-950, 2022.

[9] L. Vasquez, J. Redondo, D. Hervas, V. Ramírez., and J. Torres, "Balancing CO2 emissions and economic cost in a microgrid through an energy management system using MPC and multi-objective optimization," *Applied Energy*, vol. 347, no. 3, pp. 120998, 2023.

[10] M. Yousif, Q. Ai, Y. Gao, W. Wattoo, Z. Jiang, and R. Hao, "An optimal dispatch strategy for distributed microgrids using PSO," *CSEE Journal of Power and Energy Systems*, vol. 6, no.3, pp.724-734, 2021.

[11] J. Hou, W. Yu, Z. Xu, Q. Ge, Z. Li, and Y. Meng, "Multi-time scale optimization scheduling of microgrid considering source and load uncertainty," *Electric Power Systems Research*, vol. 216, pp. 109037, 2023.

[12] S. Li, J. Zhu, H. Dong, H. Zhu, and J. Fan, "A novel rolling optimization strategy considering grid-connected power fluctuations smoothing for renewable energy microgrids," *Applied Energy*, vol. 309, pp. 118441, 2022.

[13] A. Khalil, T. Boghdady, M. Alham, and D. Ibrahim, "Enhancing the conventional controllers for load frequency control of isolated microgrids using proposed multi-objective formulation via artificial rabbits optimization algorithm, *IEEE Access*, vol. 11, pp. 3472-3493, 2022.

[14] Y. Dong, F. Liu, X. Lu, Y. Lou, Y. Ma, N. Eghbalian, " Multi-objective economic environmental energy management microgrid using hybrid energy storage implementing and developed manta ray foraging optimization algorithm," *Electric Power Systems Research*, vol. 211, pp. 108181, 2022.

[15] A. Bukara, C. Tana, L. Yiew, R. Ayop, and W. Tan, "A rule-based energy management scheme for long-term optimal capacity, planning of grid-independent microgrid optimized by multi-objective grasshopper optimization algorithm," *Energy Conversion and Management*, vol. 221, pp. 113161, 2020.